ACS Catalysis

pubs.acs.org/acscatalysis

Research Article

Influence of Adhesion on the Chemical Potential of Supported Nanoparticles as Modeled with Spherical Caps

Philipp N. Plessow* and Charles T. Campbell

Cite This: ACS Catal. 2022, 12, 2302−2308

Read Online

ACCESS | Metrics & More | Article Recommendations | Supporting Information

ABSTRACT: The effect of adhesion on the chemical potential of supported nanoparticles is derived for the case of spherical caps. It is explicitly shown that for the minimum-energy particle shape (neglecting any anisotropy in surface energy), the chemical potential of a spherical cap attached to any flat support material reduces to $\mu = 2\gamma V_m/r$, where r is the radius of curvature, γ is the surface energy, and V_m is the volume per mole of atoms. This is identical to the well-known Gibbs−Thomson relation derived instead for free-standing spherical particles. The chemical potential nevertheless depends on the adhesion energy E_{adh} because this radius r is a strong function of both adhesion (specifically, of E_{adh}/γ) and particle volume. The approximation of hemispherical particle shape, for which $\mu = (3\gamma - E_{adh})V_m/r$ as proposed by Campbell and Hemmingson (*ACS Nano* **2017, 11,** 1196) is exact for $\gamma = E_{adh}$, where it reduces to $\mu = 2\gamma V_m/r$. Using hemispheres, or any fixed particle shape, is furthermore shown to be a linear approximation to the exact dependence of μ on E_{adh} for the minimum-energy particle shape, with error <10% for contact angles between 66 and 120° (i.e., for $E_{adh}/\gamma = 0.5-1.4$). Generally, these approaches only consider the limit of a large radius of curvature, where γ and E_{adh} are constant. It is known that both γ and E_{adh} increase with the decreasing r below 4 nm.

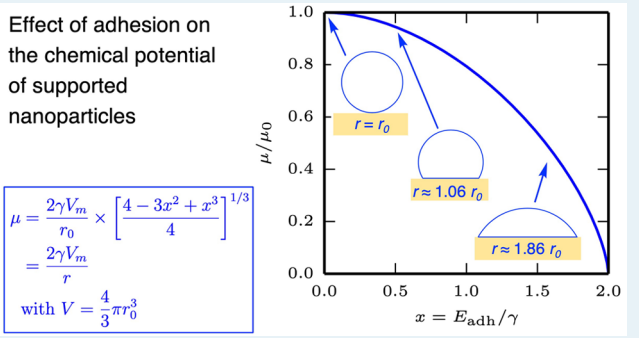

KEYWORDS: *nanoparticles, chemical potential, sintering, adhesion, metal-support interaction*

INTRODUCTION

The stability of metal nanoparticles plays an important role both in the synthesis as well as in the stability of heterogeneous catalysts. With increasing size, metal particles generally become more stable and the metal atom chemical potential approaches that of the bulk metal. This trend in stability can be attributed to the ratio of the surface area to volume (or number of atoms), which is higher for small particles. This situation provides a thermodynamic driving force for small particles to sinter to larger particles. On the other hand, the high surface area of small particles is generally a desirable property for catalysis because it leads to higher overall activity, in the absence of other particle size effects. For this reason, sintering of nanoparticles that form an active catalyst is generally a process that is sought to be avoided.[1−3] This is even more important for some catalyst materials like Au, where the activity per unit area decreases strongly with the increasing size above 2 nm.[4]

The most important problem with sintering is its inhibiting effect on the development of new industrial catalysts for the production of fuels and commodity chemicals, the clean combustion of fuels and vehicle exhaust cleanup. To be practical, these types of catalysts often need to remain on-stream for times of nearly a year or more before replacement. Thus, every time a promising new catalyst material is discovered, it must be tested for a year to determine if it deactivates by sintering. This greatly slows down the development of better industrial catalysts. Thus, for new catalyst development, there is a tremendous practical motivation to develop theoretical methods that can predict long-term catalyst sintering behavior based on short-term measurements. It is well known that the chemical potential (μ) of metal atoms in nanoparticles depends sensitively on the particle size and support material upon which it is anchored and that it is a key parameter required for any quantitative kinetic model that could predict such sintering rates.[5,6] We present here new insights into how this chemical potential depends on the nanoparticle size and support material.

This chemical potential enters into many rate equations for catalyst sintering, where it approximately enters as a negative contribution to the activation energy for sintering.[7−10] The

Received: October 8, 2021
Revised: December 29, 2021
Published: January 31, 2022

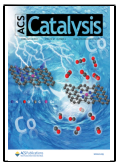

chemical potential also serves as a descriptor for the chemical reactivity of the metal atoms at the surface of a catalyst. The higher the chemical potential, the more strongly the metal atoms bind to small adsorbates like −OH and $-CH_3$.[5,6] Thus, there is a strong motivation to achieve a quantitative description of how chemical potential varies with the particle size and support material.

Catalyst nanoparticles are generally supported, often on an oxide, carbon, or a nitride, and the choice of this support material provides a degree of freedom that can be utilized effectively to suppress sintering and increase particle stability. The support material may directly influence the kinetics of sintering, for example, for surface-mediated Ostwald ripening, where metal atoms diffuse over the support.[11−18] More generally, however, the metal/support interface influences the stability of the nanoparticles.

For a theoretical, quantitative description of the stability of supported particles, two general approaches exist. One is explicit modeling or simulation of supported particles. This approach is computationally very demanding and is, when based on the density functional theory, usually explored only for relatively small systems.[19−22] Larger systems were also investigated,[23,24] but here, it is not viable to systematically explore many local minima to obtain a reasonable estimate of the global minimum.

The second approach relies on a continuum description of the particle, where atoms in the bulk have the bulk chemical potential μ_{bulk} and surfaces increase the total energy by the product of surface area and surface energy γ. For free-standing crystalline particles, surface energies generally depend on the facet orientation and the minimum energy particle shape is given by the Wulff construction,[25] which is then modified upon adhesion to a foreign support surface.[26,27] The bonding interaction with the support is expressed through the adhesion energy per surface area, E_{adh}. Generally, the Wulff construction and its modification through adhesion to a support therefore require knowledge about the stability of all relevant facets. For example, clean metal fcc particles typically expose the fcc(111) and fcc(100) surfaces. However, in the presence of adsorbates such as oxygen, higher-index facet become more stable and the particle can then become more rounded.[28]

If the surface energy is independent of facet orientation, the minimum particle shape is given by a sphere in the absence of adhesion and by a spherical cap in the presence of adhesion. This is the case for liquids, which have no facets, but the approximation is also often applied to solid particles. The chemical potential of free-standing spherical particles is given by the Gibbs−Thomson relation[11,29,30]

$$\mu = \frac{2\gamma V_m}{r} \tag{1}$$

where r is the particle radius and V_m is the volume per atom. Both the Wulff-construction and the Gibbs−Thomson relation lead to the same functional behavior, $\mu \propto 1/r$ (or, equivalently, $\mu \propto V^{-1/3}$). Because the surface energy (or energies) are often used as an adjustable parameter that is fitted to the experiment, both approaches can lead to the same result upon fitting. Compared to the Wulff-construction, the Gibbs−Thomson relation has the advantages of having a simple functional form and of depending only on a single parameter. The Gibbs−Thomson relation is therefore convenient to use when no detailed knowledge on the facet dependence of γ is available, which is common because experimental values for γ are usually only measured for flat polycrystalline but annealed surfaces, which are dominated by the lowest-energy facet.

Although it has been noted, for example, by Wynblatt and Gjostein[11] that μ given by the Gibbs−Thomson relation "is independent of θ" (θ being the contact angle), it is not obvious how the chemical potential depends on adhesion. Hemispherical particles have also been used to describe the chemical potential of supported nanoparticles, where Campbell and Hemmingson[31] have derived the relation

$$\mu = (3\gamma - E_{adh})\left(\frac{V_m}{r}\right) \tag{2}$$

that explicitly depends on the adhesion energy E_{adh}. This equation assumed that the values of γ and E_{adh} were constant at their large-particle-size limits. An empirical correction factor of $[1 + (0.75\ \text{nm/r})]$ was later added to this equation to approximately account for the fact that these increase strongly with the decreasing r below ∼4 nm.[5,6] The goal of this present work is to explore the general dependence of μ on E_{adh} and r for spherical caps with any contact angle and, specifically, with minimum energy shape.

RESULTS AND DISCUSSION

This work is organized as follows: we will first discuss the general shape of spherical caps and the involved quantities. Starting from the total energy, we will then derive the chemical potential and from that the chemical potential of the minimum energy particle shape. Lastly, the effect of adhesion will be analyzed and compared to the model of hemispherical particles.

Total Energy of a Spherical Cap with Adhesion. Spherical caps on surfaces can generally be categorized by the height h that is cut off from the corresponding full sphere with radius r. Henceforth, we will refer to this r as the radius of curvature. We will use the ratio

$$x = \frac{h}{r} \tag{3}$$

as a general size-independent measure of the particle shape. As illustrated in Figure 1a, for $0 \le x \le 1$, the particle is in between a sphere and a hemisphere. For $1 < x \le 2$, the particle is in between a hemisphere and a thin film, that is formed in the limit of complete wetting. Figure 1 also shows the apparent

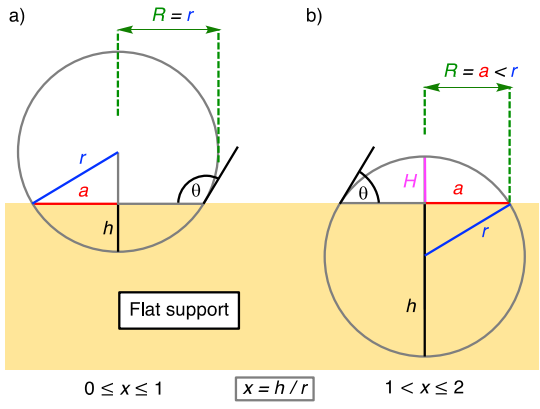

Figure 1. Illustration of the quantities occurring for a spherical cap describing a particle for adhesion leading to (a) $h \le r$ and (b) $r < h \le 2r$. The contact angle θ is also indicated, and $a = r \sin \theta$.

https://doi.org/10.1021/acscatal.1c04633
ACS Catal. 2022, 12, 2302−2308

radius R that is obtained by projecting the spherical cap on the support area. Importantly, for $x < 1$, R and r are equal, while for $x > 1$, we find $R < r$.

The particle/support interface area and total surface area are given by

$$A_{\text{interface}} = \pi r^2(2x - x^2) \tag{4}$$

$$A_{\text{total}} = \pi r^2(4 - x^2) \tag{5}$$

The total energy can now be calculated based on the surface energy γ and the adhesion energy E_{adh}, where we use the convention that binding adhesion is positive. We are only interested in the extra energy that exceeds the energy per mole for the bulk solid (or liquid) at infinite particle size. This energy arises due to surface energy and interfacial adhesion energy. We limit our derivation to particles with the same number of atoms (i.e., constant volume) and investigate the effect of adhesion on the energy. We thus use $E = E_{\text{surface}} = E_{\text{tot}} - E_{\text{bulk}}$

$$E = \gamma \times A_{\text{total}} - E_{\text{adh}} \times A_{\text{interface}} \tag{6}$$

Inserting the areas from eqs 4 and 5 gives

$$E = \pi r^2[\gamma \times (4 - x^2) - E_{\text{adh}} \times (2x - x^2)] \tag{7}$$

Chemical Potential of a Particle with Fixed Particle Shape. We now reformulate the size dependency in terms of number of moles of atoms (n) and molar volume (V_{m}), as in ref 31. As mentioned above, we consider only the surface energy, which means that the chemical potential μ that we derive is given relative to the bulk chemical potential in an infinite-size particle: $\mu = \mu_{\text{tot}} - \mu_{\text{bulk}}$:

Calculating the chemical potential by ignoring the small variation with particle size in the entropic contribution to free energy, as in ref 31, we have

$$\mu = \left(\frac{\partial E}{\partial n}\right)_{x,\gamma,E_{\text{adh}}} \tag{8}$$

Substituting eq 7 for E, we arrive at (see Appendix for details)

$$\mu = \frac{2\gamma V_{\text{m}}}{r} \times \frac{(4 - x^2) - \frac{E_{\text{adh}}}{\gamma} \times (2x - x^2)}{4 - 3x^2 + x^3} \tag{9}$$

Equation 9 is the final expression of the chemical potential for a given particle shape. For $x = 0$, it reduces to the Gibbs–Thomson equation (eq 1); for $x = 1$, it reduces to the formula given by Campbell and Hemmingson for hemispherical shape[31] (eq 2).

Chemical Potential of a Particle with Optimal Particle Shape. In order to determine the optimum particle shape (neglecting any anisotropy in surface energy), we locate the minimum of E with respect to x, which is identical to the minimum of μ with respect to x at constant n (or constant V) rather than constant r. Using the volume of the particle (see Appendix) and $V = nV_{\text{m}}$ and

$$r = \left[\frac{3V}{\pi(4 - 3x^2 + x^3)}\right]^{1/3} \tag{10}$$

we obtain

$$\mu = 2\gamma\left[\frac{\pi V_{\text{m}}^2}{3n}\right]^{1/3} \times \frac{(4 - x^2) - \frac{E_{\text{adh}}}{\gamma} \times (2x - x^2)}{(4 - 3x^2 + x^3)^{2/3}} \tag{11}$$

and determine the first derivative of μ with respect to x

$$\left(\frac{\partial \mu}{\partial x}\right)_{n,\gamma,E_{\text{adh}}} = 2\gamma\left[\frac{\pi V_{\text{m}}^2}{3n}\right]^{1/3} \times \frac{2\left(x - \frac{E_{\text{adh}}}{\gamma}\right)}{(x + 1) \times [(x - 2)^2(x + 1)]^{2/3}} \tag{12}$$

This derivative is zero for the minimum energy (most stable) shape. From the numerator in eq 12, we can directly read off the root that $x = E_{\text{adh}}/\gamma$. This means that, in the equilibrium shape, $x = h/r$ is simply equal to E_{adh}/γ.

This is consistent with the well-known result for the equilibrium shape, whereby $E_{\text{adh}}/\gamma = 1 + \cos\theta$ where θ is the contact angle.[32] As seen in Figure 1, $x = h/r = 1 + \cos\theta$, which equals E_{adh}/γ. If we now substitute $E_{\text{adh}}/\gamma = x$ into eq 11, it gives

$$\mu = \frac{2\gamma V_{\text{m}}}{r} \times \underbrace{\left(\frac{(4 - x^2) - x(2x - x^2)}{4 - 3x^2 + x^3}\right)}_{=1} \tag{13}$$

where the entire x-dependent part reduces to one, thus giving us the final result

$$\mu = \frac{2\gamma V_{\text{m}}}{r} \tag{14}$$

This is somewhat surprisingly the same equation as the Gibbs–Thomson relation for a free-standing particle, already shown in eq 1. We discuss next the role of the adhesive contact between the particle and the support, which is absent from this equation as written, but nevertheless true for supported particles as well. We show that the adhesion energy dictates the particle's radius of curvature (r) for a given volume and thus strongly affects the chemical potential at fixed volume.

Role of Adhesion. Equation 14 is identical to the so-called Gibbs–Thomson equation and is therefore obviously correct in the limit of no adhesion, where $x = 0$ and $E_{\text{adh}} = 0$. It is also correct in the limit investigated by Campbell and coworkers, for hemispheres, which are the equilibrium particle shape for $E_{\text{adh}} = \gamma$. Here, for the formula given by Campbell (eq 2)

$$\mu = (3\gamma - E_{\text{adh}})\left(\frac{V_{\text{m}}}{r}\right) \tag{15}$$

if we insert $E_{\text{adh}} = \gamma$, it gives again eq 14. This result may seem puzzling because it seems to imply that the support and adhesion have no effect. However, the effect of adhesion comes through determining the equilibrium radius of curvature for a given volume particle. This radius (r) is a function of adhesion ($x = E_{\text{adh}}/\gamma$) and volume (or, equivalently, number of atoms n). Qualitatively, stronger adhesion will—at constant number of atoms or volume—lead to a larger radius and therefore a lower chemical potential. Still, this means that, within the assumption of sphere-derived particles, a particle with a given radius r has the same chemical potential on any support. However, it is important to differentiate between the radius r that refers to the radius of the sphere from which the cap is derived and the apparent (projected) radius R that may be observed in an experiment (see the Supporting Information for a more

https://doi.org/10.1021/acscatal.1c04633
ACS Catal. 2022, 12, 2302−2308

detailed discussion of particles with constant apparent radius R).

Figure 2 shows the chemical potential of a spherical cap with constant volume as a function of E_{adh}/γ. In the absence of

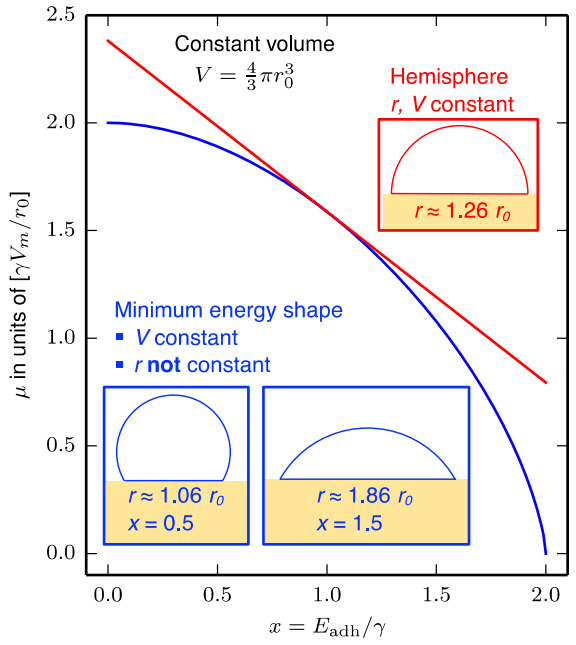

Figure 2. Blue curve: chemical potential of a particle with the fixed number of atoms n, which is identical to fixed volume $V = (4/3)\pi r_0^3$, as a function of adhesion, E_{adh}/γ, for the minimum-energy (equilibrium) shape, from eq 18. The chemical potential is given in units of $[\gamma V_m/r_0]$, where r_0 is the radius of a spherical particle of the same volume. The equilibrium radius r changes as a function of E_{adh}/γ, and the depicted chemical potential is always equal to $2\gamma V_m/r$ with the respective r. Red line: chemical potential assuming the hemispherical particle shape, which is not the equilibrium shape.

adhesion, the most stable shape is a sphere with radius r_0 and chemical potential

$$\mu(\text{sphere}) = \frac{2\gamma V_m}{r_0} \tag{16}$$

For constant V, as adhesion increases, the radius increases. Finally, for $E_{adh}/\gamma = 1$, we arrive at the half-spherical shape with $r = r_0 \times 2^{1/3} \approx r_0 \times 1.26$, with a chemical potential of

$$\mu(\text{hemisphere}) = \frac{2\gamma V_m}{r} = \frac{2\gamma V_m}{r_0} \times 2^{-1/3} \approx \frac{1.58 \times \gamma V_m}{r_0} \tag{17}$$

Generally, substituting the radius r in the Gibbs−Thomson relation (eq 1) again with eq 10 and expressing the constant volume $V = 4/3\pi r_0^3$ in terms of the radius of the sphere r_0, we get

$$\mu = \frac{2\gamma V_m}{r_0} \times \left[\frac{4 - 3x^2 + x^3}{4}\right]^{1/3} \text{ with } x = \frac{E_{adh}}{\gamma} \tag{18}$$

which nicely shows the relation to the Gibbs−Thomson relation as formulated with a variable radius r. When given relative to the chemical potential of a sphere with radius r_0, adhesion is seen to modify μ with a function $f(x)$ that varies between $f(0) = 1$ and $f(2) = 0$. Alternatively, one can formulate μ directly in terms of the total particle volume V

$$\mu = \frac{2\gamma V_m}{V^{1/3}} \times \left[\pi\frac{4 - 3x^2 + x^3}{3}\right]^{1/3} \text{ with } x = \frac{E_{adh}}{\gamma} \tag{19}$$

Equation 19 transparently shows size and adhesion dependence of the chemical potential. For increasing adhesion at constant V, we find $\lim_{x\to 2}\mu(x,V) = 0$ and $\lim_{x\to 2} r(x,V) = \infty$, which means that a thin film is formed and that the chemical potential μ becomes identical to the bulk chemical potential ($\mu = 0$). This corresponds to the situation of a metal particle deposited on a flat surface of the same metal. The dependence of the chemical potential on adhesion for a particle with constant volume is shown in Figure 2.

Figure 2 shows that μ(hemisphere) is a tangent to μ for particles with the minimum energy shape at $x = 1$, where hemispheres are the minimum energy shape. This means that μ(hemisphere) can be considered a first-order approximation around $x = 1$. This can be generalized to any fixed-particle shape. Taking the first derivative of the chemical potential for the optimal particle shape (eq 19) with respect to $x = E_{adh}/\gamma$ gives

$$\left(\frac{\partial\mu}{\partial x}\right)_{V,\gamma} = 2\gamma V_m\left[\frac{\pi}{3V}\right]^{1/3} \times \frac{x^2 - 2x}{(4 - 3x^2 + x^3)^{2/3}} \tag{20}$$

The chemical potential for the fixed particle shape $x = h/r$ (eq 11) can be seen to depend linearly on E_{adh}, which is due to the fact that the particle/support interface area remains constant for the fixed particle shape. The partial derivative of eq 11 with respect to E_{adh}/γ at constant γ is identical to eq 20. This shows that the chemical potential of the spherical cap with a fixed particle shape $x = h/r$ is not only identical to the minimum energy shape at $x = E_{adh}/\gamma$ but can also be considered a linear approximation to the variation of μ with E_{adh}.

Besides the absolute value of the chemical potential, its variation with particle size is also important, as it determines the driving force for sintering. The dependence of μ on size is given in Figure 3 as a function of $V^{-1/3}$, which gives a linear relationship. This shows that the variation of the chemical potential with particle size, as measured through the volume or

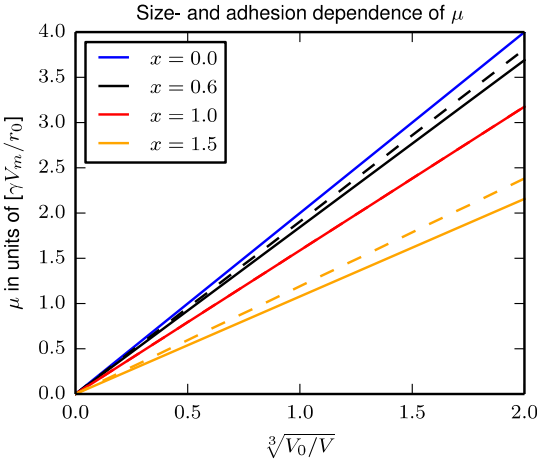

Figure 3. Dependence of the chemical potential on particle size ($V^{-1/3}$) for varying adhesion, $x = E_{adh}/\gamma$. Results for hemispherical particles are indicated with a dashed line for $x = 0.6$ and $= 1.5$. For $x = 1.0$, this is identical to the minimum energy shape shown with a solid line.

https://doi.org/10.1021/acscatal.1c04633
ACS Catal. 2022, 12, 2302−2308

number of atoms, is reduced with the increasing x. Therefore, in agreement with general expectations, stronger adhesion leads to a weaker driving force for sintering. Figure 3 also shows that approximating particles as hemispheres generally overestimates the variation of μ with particle size, except at x = 1, where the approximation is exact.

Finally, it is interesting to study the effect of adhesion on μ for a few specific examples. Using the data for γ and E_{adh} compiled in ref 31 and the corresponding values for V_m (see also Table S1), the chemical potentials for hemispherical and minimum energy shapes calculated using eq 18 are shown in Figure 4.

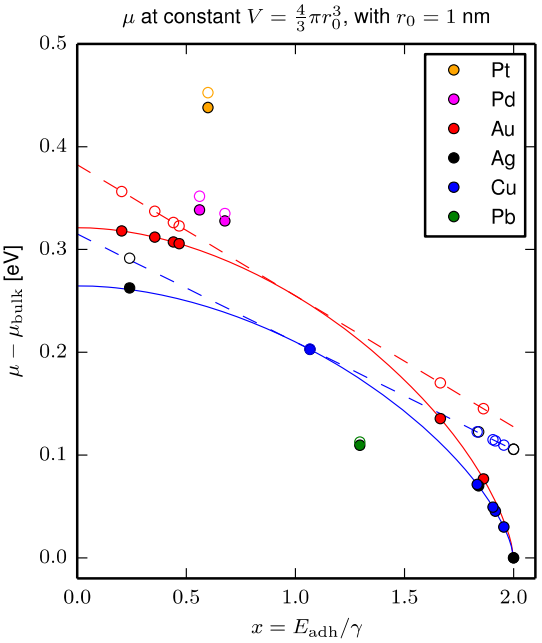

Figure 4. Calculated chemical potential for particles of constant volume (equal to that for a sphere of radius r_0 = 1 nm) using eq 18 with experimentally determined values of γ and E_{adh} for various supports [MgO(100), TiO_2(110), $CeO_{1.8}$(111), $CeO_{1.9}$(111), $CeO_{1.95}$(111), Fe_3O_4(111), and α-Al_2O_3(0001)] and metals from ref 31. Filled symbols show the chemical potential as computed for the minimum energy particle shape, and hollow symbols correspond to hemispherical-shaped particles. For Cu and Au, μ is shown additionally as a continuous function of x (dashed for hemispheres).

When E_{adh} Exceeds 2γ: Complete Wetting. For completeness, we also consider the case when E_{adh} exceeds 2γ and the material wets the support to make a continuous thin film of thickness t. In that case

$$A_{interface} = n(V_m/t) \tag{21}$$

and

$$E = (2\gamma - E_{adh}) \times A_{interface} = (2\gamma - E_{adh})n(V_m/t) \tag{22}$$

The chemical potential is then

$$\mu = \left(\frac{\partial E}{\partial n}\right)_{t,E_{adh}} = (2\gamma - E_{adh})(V_m/t) \tag{23}$$

This is a negative value whose magnitude decreases with t proportional to $1/t$. Such complete wetting often arises when late transition metals adsorb onto the surfaces of earlier transition metals.[33]

Implications Regarding Sintering Kinetic Models. Perhaps the most important pioneering paper about sintering kinetics of supported nanoparticle catalysts was the extensive series of derivations presented by Wynblatt and Gjostein (W−G),[13] which have been widely used in modeling of sintering kinetics.[7−10,34,35]

In the part of that W−G paper about sintering via the Ostwald-ripening mechanism, they used the Gibbs−Thomson relation, eq 1, which we have proven above is appropriate even when the adhesion energy between the particle and the support is strong, because eq 14 is identical to eq 1, although derived for the more general case that considers adhesion. As noted above, E_{adh} manifests itself only through the contact angle θ. The effect was well modeled by Wynblatt and Gjostein through their geometrical factor α_1 equal to $(2 - 3\cos\theta + \cos^3\theta)/4$, which is the ratio of the particle volume to that of a full sphere with the same radius of curvature: $V = 4/3\ \pi R^3\ \alpha_1$. As adhesion gets stronger, the contact angle gets smaller, α_1 gets smaller, and the radius increases for fixed volume, and so, the chemical potential drops. These effects are all still accurately represented in the classic Wynblatt−Gjostein equations.

However, there are two important corrections that need to be considered when using the Wynblatt−Gjostein equations. Those equations were derived using this Gibbs−Thomson relation for μ, assuming that γ is independent of size and neglecting all but the first-order terms in a Taylor series expansion of $\exp[\mu/(RT)]$, where R is the gas constant and T is the temperature. We have shown that both of these simplifications are problematic and lead to substantial errors.[8,10]

Most recently, we have shown that γ for late transition metals increases with the decreasing r approximately proportional to $[1 + (0.75\ \text{nm})/r]$, thus doubling from the bulk value when r drops to 0.75 nm.[5,6] Both of these effects must be included when using the Wynblatt−Gjostein equations to achieve the best accuracy in sintering rate predictions.

Summary and Conclusions. The chemical potential of metal atoms in supported nanoparticles with the shape of spherical caps in the presence of adhesion has been derived. The most stable shape of a spherical cap can be described in terms of the ratio of adhesion energy per surface area to surface energy, $x = E_{adh}/\gamma = 1 + \cos\theta$. Starting from a sphere with a height of $d = 2r$, a segment with the height h is cut off due to adhesion, leaving a spherical cap with shape $h/r = x$. Thus, for ratios of $0 < E_{adh}/\gamma < 2$, the particle shape varies in between a sphere and a thin film. At constant r, the height of the particle varies linearly with $x = E_{adh}/\gamma$. The most stable shape is a hemisphere only for the special case where $E_{adh} = \gamma$ (i.e., x = 1).

For the minimum-energy particle shape, it was proven here that the chemical potential is given by $\mu = 2\gamma V_m/r$, which is the same equation as the Gibbs−Thomson relation for free-standing spheres. The chemical potential thus depends only on the radius of curvature of the particle, r. However, the chemical potential for particles of constant volume (or number of atoms) at their lowest-energy shape depends strongly on adhesion (i.e., on $x = E_{adh}/\gamma$) because r depends strongly on x for that case (as given by eq 40 in the Appendix).

Describing a particle's chemical potential assuming the hemispherical shape is a reasonable first-order approximation around $x = E_{adh}/\gamma = 1$. For example, as shown in Figure 4, the error is <10% when x is between 0.5 and 1.4 (i.e., when θ is between 66 and 120°). When θ approaches 0 (wetting), the error in that approximation gets very large and one must

https://doi.org/10.1021/acscatal.1c04633
ACS Catal. 2022, 12, 2302−2308

accurately consider the shape. One must also consider the fact that both γ and E_{adh} increase with the decreasing r below 4 nm and are only truly constant for large r.[5,6]

APPENDIX

Surface Areas

The circular interface area for weak adhesion (Figure 1) is given by

$$A_{interface} = \pi a^2 \tag{24}$$

$$A_{interface} = \pi(r^2 - (r-h)^2) \tag{25}$$

$$A_{interface} = 2\pi rh - \pi h^2 \tag{26}$$

The exposed surface area is given by the difference of the area of a sphere ($A = 4\pi r^2$) and the area of the curved part of the cut-off spherical cap ($A = 2\pi rh$)[36]

$$A_{exposed} = 4\pi r^2 - 2\pi rh \tag{27}$$

The total surface area (including interface) is given by

$$A_{total} = A_{exposed} + A_{interface} \tag{28}$$

$$A_{total} = 4\pi r^2 - \pi h^2 \tag{29}$$

Substituting $x = h/r$ into eqs 26 and 29 gives eqs 4 and 5.

For strong adhesion leading to $h > r$, the same formulas as shown above apply. Here, the spherical cap is smaller than a hemisphere and has the height H, which is related to the quantity h as follows

$$H = 2r - h \tag{30}$$

The interface area is given by

$$A_{interface} = \pi a^2 \tag{31}$$

$$A_{interface} = \pi(r^2 - (r-H)^2) \tag{32}$$

$$A_{interface} = 2\pi rH - \pi H^2 \tag{33}$$

$$A_{interface} = 2\pi r(2r-h) - \pi(2r-h)^2 \tag{34}$$

$$A_{interface} = 2\pi rh - \pi h^2 \tag{35}$$

which is identical to eq 26. The exposed surface area is given by

$$A_{exposed} = 2\pi rH \tag{36}$$

$$A_{exposed} = 4\pi r^2 - 2\pi rh \tag{37}$$

which is identical to eq 27. Therefore, the same formulas for the surface can be used for $0 < h < 2r$.

Chemical Potential

The volume of the particle is given by the difference between that of a sphere ($V = 4/3\pi r^3$) and that of the cut-off spherical cap [$V = 1/3\pi(3rh^2 - h^3)$][36]

$$V = \frac{1}{3}\pi(4r^3 - 3rh^2 + h^3) \tag{38}$$

$$V = \frac{1}{3}\pi r^3(4 - 3x^2 + x^3) \tag{39}$$

We note the similarity with the α_1 parameter in the work of Wynblatt and Gjostein.[13] We now equate this with $V = V_m \times n$ and solve for r

$$r = \left[\frac{3V_m}{\pi(4 - 3x^2 + x^3)}\right]^{1/3} n^{1/3} \tag{40}$$

Using eq 7, the total energy is now expressed as

$$E = \pi n^{2/3}\left[\frac{3V_m}{\pi(4 - 3x^2 + x^3)}\right]^{2/3}[\gamma(4 - x^2) - E_{adh}(2x - x^2)] \tag{41}$$

We can now calculate the chemical potential by taking the derivative of E with respect to n, according to eq 8

$$\mu = \frac{2\pi}{3} n^{-1/3}\left[\frac{3V_m}{\pi(4 - 3x^2 + x^3)}\right]^{2/3}[\gamma(4 - x^2) - E_{adh}(2x - x^2)] \tag{42}$$

Using eq 40 we now express n back in terms of r:

$$\mu = \frac{2\pi}{3} r^{-1}\left[\frac{3V_m}{\pi(4 - 3x^2 + x^3)}\right][\gamma(4 - x^2) - E_{adh}(2x - x^2)] \tag{43}$$

and obtain eq 9.

ASSOCIATED CONTENT

Supporting Information

The Supporting Information is available free of charge at https://pubs.acs.org/doi/10.1021/acscatal.1c04633.

Additional information for the chemical potential of spherical caps with constant apparent radius and tabulated data used in Figure 4 (PDF)

AUTHOR INFORMATION

Corresponding Author

Philipp N. Plessow − *Institute of Catalysis Research and Technology, Karlsruhe Institute of Technology, Eggenstein-Leopoldshafen 76344, Germany;* orcid.org/0000-0001-9913-4049; Email: philipp.plessow@kit.edu

Author

Charles T. Campbell − *Department of Chemistry, University of Washington, Seattle, Washington 98195-1700, United States;* orcid.org/0000-0002-5024-8210

Complete contact information is available at: https://pubs.acs.org/10.1021/acscatal.1c04633

Author Contributions

The manuscript was written through contributions of all authors. All authors have given approval to the final version of the manuscript.

Notes

The authors declare no competing financial interest.

ACKNOWLEDGMENTS

P.N.P. acknowledges financial support from the Helmholtz Association and funding by the Deutsche Forschungsgemeinschaft (DFG, German Research Foundation)—SFB 1441—

Project-ID 426888090. C.T.C. acknowledges financial support from the U. S. Department of Energy, Office of Basic Energy Sciences, Chemical Sciences Division grant no DE-FG02-96ER14630. The authors thank Nida Janulaitis for proof-reading the manuscript.

REFERENCES

(1) Dai, Y.; Lu, P.; Cao, Z.; Campbell, C. T.; Xia, Y. The physical chemistry and materials science behind sinter-resistant catalysts. *Chem. Soc. Rev.* **2018**, *47*, 4314−4331.
(2) Wang, L.; Wang, L.; Meng, X.; Xiao, F. S. New Strategies for the Preparation of Sinter-Resistant Metal-Nanoparticle-Based Catalysts. *Adv. Mater.* **2019**, *31*, No. e1901905.
(3) Goodman, E. D.; Schwalbe, J. A.; Cargnello, M. Mechanistic Understanding and the Rational Design of Sinter-Resistant Heterogeneous Catalysts. *ACS Catal.* **2017**, *7*, 7156−7173.
(4) Valden, M.; Lai, X.; Goodman, D. W. Onset of catalytic activity of gold clusters on titania with the appearance of nonmetallic properties. *Science* **1998**, *281*, 1647−1650.
(5) Mao, Z.; Campbell, C. T. Predicting a Key Catalyst-Performance Descriptor for Supported Metal Nanoparticles: Metal Chemical Potential. *ACS Catal.* **2021**, *11*, 8284−8291.
(6) Campbell, C. T.; Mao, Z. Chemical Potential of Metal Atoms in Supported Nanoparticles: Dependence upon Particle Size and Support. *ACS Catal.* **2017**, *7*, 8460−8466.
(7) Rahmati, M.; Safdari, M.-S.; Fletcher, T. H.; Argyle, M. D.; Bartholomew, C. H. Chemical and Thermal Sintering of Supported Metals with Emphasis on Cobalt Catalysts During Fischer-Tropsch Synthesis. *Chem. Rev.* **2020**, *120*, 4455−4533.
(8) Farmer, J. A.; Campbell, C. T. Ceria Maintains Smaller Metal Catalyst Particles by Strong Metal-Support Bonding. *Science* **2010**, *329*, 933−936.
(9) Houk, L. R.; Challa, S. R.; Grayson, B.; Fanson, P.; Datye, A. K. The definition of ″critical radius″ for a collection of nanoparticles undergoing Ostwald ripening. *Langmuir* **2009**, *25*, 11225−11227.
(10) Parker, S. C.; Campbell, C. T. Kinetic model for sintering of supported metal particles with improved size-dependent energetics and applications to Au onTiO2(110). *Phys. Rev. B: Condens. Matter Mater. Phys.* **2007**, *75*, 035430.
(11) Wynblatt, P.; Gjostein, N. A. Particle growth in model supported metal catalysts—I. Theory. *Acta Metall.* **1976**, *24*, 1165−1174.
(12) Wynblatt, P. Particle growth in model supported metal catalysts—II. Comparison of experiment with theory. *Acta Metall.* **1976**, *24*, 1175−1182.
(13) Wynblatt, P.; Gjostein, N. A. Supported metal crystallites. *Prog. Solid State Chem.* **1975**, *9*, 21−58.
(14) Chu, Y.; Ruckenstein, E. On the sintering of platinum on alumina model catalyst. *J. Catal.* **1978**, *55*, 281−298.
(15) Ruckenstein, E.; Pulvermacher, B. Growth kinetics and the size distributions of supported metal crystallites. *J. Catal.* **1973**, *29*, 224−245.
(16) Ruckenstein, E.; Dadyburjor, D. B. Mechanisms of Aging of Supported Metal-Catalysts. *J. Catal.* **1977**, *48*, 73−86.
(17) Hansen, T. W.; DeLaRiva, A. T.; Challa, S. R.; Datye, A. K. Sintering of Catalytic Nanoparticles: Particle Migration or Ostwald Ripening? *Acc. Chem. Res.* **2013**, *46*, 1720−1730.
(18) Ruckenstein, E.; Pulvermacher, B. Kinetics of Crystallite Sintering during Heat-Treatment of Supported Metal-Catalysts. *AIChE J.* **1973**, *19*, 356−364.
(19) Tosoni, S.; Pacchioni, G. Oxide-Supported Gold Clusters and Nanoparticles in Catalysis: A Computational Chemistry Perspective. *ChemCatChem* **2018**, *11*, 73−89.
(20) Tosoni, S.; Pacchioni, G. Trends in Adhesion Energies of Gold on MgO(100), Rutile TiO_2(110), and CeO_2(111) Surfaces: A Comparative DFT Study. *J. Phys. Chem. C* **2017**, *121*, 28328−28338.
(21) Chen, H.-Y. T.; Tosoni, S.; Pacchioni, G. Adsorption of Ruthenium Atoms and Clusters on Anatase TiO2 and Tetragonal ZrO2(101) Surfaces: A Comparative DFT Study. *J. Phys. Chem. C* **2014**, *119*, 10856−10868.
(22) Zhai, H.; Alexandrova, A. N. Local Fluxionality of Surface-Deposited Cluster Catalysts: The Case of Pt7 on Al2O3. *J. Phys. Chem. Lett.* **2018**, *9*, 1696−1702.
(23) Suchorski, Y.; Kozlov, S. M.; Bespalov, I.; Datler, M.; Vogel, D.; Budinska, Z.; Neyman, K. M.; Rupprechter, G. The role of metal/oxide interfaces for long-range metal particle activation during CO oxidation. *Nat. Mater.* **2018**, *17*, 519−522.
(24) Kozlov, S. M.; Aleksandrov, H. A.; Goniakowski, J.; Neyman, K. M. Effect of MgO(100) support on structure and properties of Pd and Pt nanoparticles with 49-155 atoms. *J. Chem. Phys.* **2013**, *139*, 084701.
(25) Wulff, G. XXV. Zur Frage der Geschwindigkeit des Wachsthums und der Auflösung der Krystallflächen. *Krystallogr. Mineral.* **1901**, *34*, 449−530.
(26) Winterbottom, W. L. Equilibrium shape of a small particle in contact with a foreign substrate. *Acta Metall.* **1967**, *15*, 303−310.
(27) Kaishew, R. Equilibrium shape and nucleation work of crystals on substrates. *Commun. Bulg. Acad. Sci.* **1950**, *1*, 100.
(28) Mittendorfer, F.; Seriani, N.; Dubay, O.; Kresse, G. Morphology of mesoscopic Rh and Pd nanoparticles under oxidizing conditions. *Phys. Rev. B: Condens. Matter Mater. Phys.* **2007**, *76*, 233413.
(29) Chakraverty, B. K. Grain size distribution in thin films—1. Conservative systems. *J. Phys. Chem. Solids* **1967**, *28*, 2401−2412.
(30) Johnson, C. A. Generalization of the Gibbs-Thomson Equation. *Surf. Sci.* **1965**, *3*, 429−444.
(31) Hemmingson, S. L.; Campbell, C. T. Trends in Adhesion Energies of Metal Nanoparticles on Oxide Surfaces: Understanding Support Effects in Catalysis and Nanotechnology. *ACS Nano* **2017**, *11*, 1196−1203.
(32) Adamson, A. W.; Gast, A. P. *Physical Chemistry of Surfaces*, 6th ed.; Wiley: New York, 1997; p 353.
(33) Campbell, C. T. Bimetallic Surface Chemistry. *Annu. Rev. Phys. Chem.* **1990**, *41*, 775−837.
(34) Challa, S. R.; Delariva, A. T.; Hansen, T. W.; Helveg, S.; Sehested, J.; Hansen, P. L.; Garzon, F.; Datye, A. K. Relating Rates of Catalyst Sintering to the Disappearance of Individual Nanoparticles during Ostwald Ripening. *J. Am. Chem. Soc.* **2011**, *133*, 20672−20675.
(35) Behafarid, F.; Roldan Cuenya, B. Coarsening phenomena of metal nanoparticles and the influence of the support pre-treatment: Pt/TiO2(110). *Surf. Sci.* **2012**, *606*, 908−918.
(36) Polyanin, A. D.; Manzhirov, A. V. *Handbook of Mathematics for Engineers and Scientists*; Chapman and Hall/CRC: New York, 2006; p 69.

https://doi.org/10.1021/acscatal.1c04633
ACS Catal. 2022, 12, 2302−2308